Earth and Planetary Science Letters 274 (2008) 489–498

Contents lists available at ScienceDirect

Earth and Planetary Science Letters

journal homepage: www.elsevier.com/locate/epsl

Stratified seismic anisotropy reveals past and present deformation beneath the East-central United States

Frédéric Deschamps [a,*], Sergei Lebedev [b,c], Thomas Meier [d], Jeannot Trampert [c]

[a] Institute of Geophysics, Swiss Federal Institute of Technology, ETH Hönggerberg HPP L8.1, 8093 Zürich, Switzerland
[b] Dublin Institute for Advanced Studies, Geophysics Section, 5 Merrion Square, Dublin 2, Ireland
[c] Department of Earth Sciences, Utrecht University, PO Box 80021, 3508 TA Utrecht, The Netherlands
[d] Ruhr University Bochum, Universitätsstrasse 150, NA3/165, 44780 Bochum, Germany

ARTICLE INFO

Article history:
Received 28 April 2008
Received in revised form 29 July 2008
Accepted 31 July 2008
Available online 18 September 2008

Editor: R.D. van der Hilst

Keywords:
seismic anisotropy
surface wave
stratified anisotropy
shear-wave anisotropy
lithospheric deformation

ABSTRACT

Evolution of continental lithosphere during orogenies and the following periods of relative stability is poorly understood, largely because of the lack of relevant observational constraints. Measurements of seismic anisotropy provide such constraints, but due to limitations in the resolving power of available data sets and, more generally, of various data types, detailed mapping of lithospheric anisotropy has remained elusive. Here we apply surface-wave array analysis to data from the East-central U.S. and determine the layering of azimuthal anisotropy beneath the Grenville–Appalachian orogen in the entire lithosphere–asthenosphere depth range. Combined measurements of Rayleigh-wave phase velocities along 60 interstation paths constrain phase-velocity maps with statistically significant anisotropy. Distinct anisotropy patterns in three different period ranges point to the existence of three distinct layers beneath the orogen, with different anisotropic fabric within each. We invert phase-velocity maps and, alternatively, pairs of selected measured dispersion curves for anisotropic shear-velocity structure. The results confirm that three anisotropic layers with different fabric within each are present, two in the lithosphere (30–70 km; 70–150 km depths) and another in the asthenosphere beneath (>150 km). Directions of fast wave propagation in the upper lithosphere are parallel to the Grenville and Appalachian fronts, suggesting that the region-scale anisotropy pattern reflects the pervasive deformation of the lower crust and uppermost mantle during the continental collisions. The fast-propagation azimuth within the lower lithosphere is different, parallel to the NNW direction of North America's motion after the orogeny (~160–125 Ma). This suggests that the lithosphere, 70-km thick by the end of the Appalachian orogeny, gradually thickened to the present 150-km while inheriting the fabric from the sheared asthenosphere below, as the plate moved NNW. Below 150 km, the fast-propagation direction is parallel to the present plate motion, indicating fabric due to recent asthenospheric flow. Anisotropy in narrower depth ranges beneath the region has been sampled previously. Published results (from observations of P_n and *SKS* and waveform tomography) can be accounted for and reconciled by the three-layered model of anisotropy for the lithosphere–asthenosphere depth range constrained in this study. In particular, the anisotropy we detect in the asthenosphere can account for the magnitude of *SKS*-wave splitting, with the fast wave-propagation directions inferred from *SKS* and surface-wave data also consistent, both parallel to the current plate motion.

1. Introduction

In the course of the evolution of continental lithosphere, long periods of relative stability are interrupted by episodes of intense deformation. Many Precambrian cratons appear to have deformed little since their stabilization in the Archean or Proterozoic, thanks to the high viscosity, yield strength and compositional buoyancy of the cratonic lithosphere (e.g. Sleep, 2005). Other continental units, however, have been deformed, reworked and reshaped repeatedly in the Phanerozoic.

Our understanding of the history of such deformation and the dynamics of deforming continental lithosphere is still very incomplete. Current motions of the Earth's surface in regions undergoing active deformation are now mapped in increasing detail using Global Positioning System measurements (e.g. McClusky et al., 2000; Zhang et al., 2004), and past tectonic activity can be inferred from the geological record (e.g. Dickinson, 1971). Deformation in the deep lithosphere, however, is poorly known, largely due to the insufficiency of relevant observational constraints.

Continental collisions produce broad zones of crustal deformation (Zhang et al., 2004). Whether deformation in the mantle lithosphere is

* Corresponding author.
E-mail addresses: frederic.deschamps@erdw.ethz.ch (F. Deschamps), sergei@cp.dias.ie (S. Lebedev), meier@geophysik.ruhr-uni-bochum.de (T. Meier), jeannot@geo.uu.nl (J. Trampert).

0012-821X/$ – see front matter © 2008 Elsevier B.V. All rights reserved.
doi:10.1016/j.epsl.2008.07.058

also distributed over broad areas or, instead, occurs primarily at narrow faults has been a matter of a controversy. According to one view, continuous distributed deformation does occur in the mantle lithosphere and acts to accommodate the convergence of continental blocks (Molnar, 1988; Molnar et al., 1999). According to another view, the strong mantle lithosphere is decoupled from the deforming upper crust, and convergence in orogens is accommodated by the relative motions of nearly rigid mantle-lithospheric blocks (Tapponnier et al., 2001).

Even though much of the debate is focussed on active collisions and processes that disrupt the lithosphere, an equally important issue is the post-orogenic lithospheric evolution and the dynamics of deep lithosphere at times when the crust is relatively stable and undisturbed. One important question, in particular, is whether and how the lithosphere heals after undergoing deformation in an orogeny.

Measurements of seismic anisotropy can offer the much needed information regarding the past and present deformation in the lithosphere and mantle below. Finite strain within the crust and mantle gives rise to the lattice preferred orientation (LPO) of anisotropic major minerals, in particular amphibole and olivine in the lower crust and the upper mantle, respectively. The LPO results in the directional dependence of seismic wavespeeds, or seismic anisotropy (Christensen, 1984; Nicolas and Christensen, 1987; Becker et al., 2006; Meissner et al., 2006; Tatham et al., 2008). Azimuthal anisotropy of up to a few percent (relative to the isotropic average shear or compressional speed value) has been detected beneath both continents and oceans and appears to be a common property of both the lithosphere and asthenosphere. Beneath oceans, large-scale patterns of coherent azimuthal anisotropy have been inferred from surface-wave observations, with directions of the fastest *S*-wave propagation usually parallel to the paleo-spreading direction within the lithosphere and to the current plate motion within the asthenosphere. These patterns are consistent with basic models of mantle deformation during the development of the lithosphere near a mid-ocean ridge (in the remote past) and the shearing in the asthenosphere beneath the base of the moving oceanic plate (in the near past and at present) (Forsyth, 1975; Nishimura and Forsyth, 1989; Smith et al., 2004).

On continents, higher density of seismic stations has enabled the mapping of variations in azimuthal anisotropy with high lateral resolution using teleseismic body waves, the most common approach being with measurements of *SKS*-wave splitting (Vinnik et al., 1984; Silver, 1996). Distributions of the splitting times and fast-propagation azimuths measured at stations across continents display both large- and small-scale variations (Becker et al., 2007). In some regions, the *SKS*-inferred fast-propagation azimuths vary at small scales and appear to follow tectonic trends, whereas in other regions, including eastern North America, coherent patterns extend over broad areas, characterized by fast-propagation azimuths parallel to those of the absolute plate motion (APM) (e.g. Silver, 1996; Becker et al., 2007; Fouch and Rondenay, 2006; Savage, 1999). Because of their poor vertical resolution, however, *SKS* measurements are difficult to use for constraining the depth distribution of anisotropy. Arguments have been put forward for *SKS*-sampled anisotropy to occur predominantly within the lithosphere or predominantly within the asthenosphere (Silver, 1996; Becker et al., 2007; Fouch and Rondenay, 2006; Savage, 1999; Vinnik et al., 1992; Fischer and Wiens, 1996).

Surface waves can provide the necessary vertical resolution. Continental-scale tomographic models constrained with surface-wave observations have revealed distinctly different patterns of azimuthal anisotropy within the continental lithosphere and asthenosphere (e.g., Marone and Romanowicz, 2007; Simons et al., 2002; Debayle et al., 2005; Sebai et al., 2006). The lower lateral resolution of the large-scale imaging, however, makes it difficult to map anisotropic layering at the relatively small scale of tectonic units, so that the relationship of the inferred lithospheric anisotropy to tectonic history and history of deep lithospheric deformation is often unclear and open to debate. There is no consensus, as well, regarding the occurrence of anisotropy in subcontinental asthenosphere (e.g. (Marone and Romanowicz, 2007; Debayle et al., 2005; Gaherty and Jordan, 1995; Gung et al., 2003).

Recently, data sets from dense arrays of broad-band seismic stations have been growing in both their number and size. Applications of surface-wave analysis to array data have been producing increasingly high imaging resolution, both lateral and radial (Li et al., 2003; Pedersen et al., 2006; Yang and Forsyth, 2006; Yao et al., 2006; Zhang et al., 2007; Deschamps et al., 2008). Array data enable the mapping of anisotropic layering in the lithosphere and asthenosphere at the scale of tectonic units, thus providing essential constraints on the history of continental deformation.

In this paper, we use measurements of interstation surface-wave dispersion in the East-Central U.S. and constrain the layering of azimuthal anisotropy beneath the Grenville–Appalachian orogenic region. We show that anisotropy beneath this Proterozoic–Phanerozoic orogen is different from that beneath the neighbouring cratonic platform of an older age. Three layers with different anisotropic fabric within each occur beneath the orogen and characterize successive stages of the evolution of its lithosphere.

2. East-central US: tectonic history and observations of anisotropy

The Grenville and Appalachian orogenic deformation fronts (Hoffman, 1988) cross the region sampled by our data (33°–40°N, 83°–91°E) at an approximately NE–SW azimuth (Fig. 1). The Grenville orogeny is thought to be the last episode (1.3–1.0 Ga) of a major continental accretion sequence along the southern edge of Laurentia that started about 1.8 Ga ago (Hoffman, 1988; Dalziel, 1991; Karlstrom et al., 2001). The Appalachian orogen is associated with more recent collisions at 0.42–0.27 Ga (Ziegler, 1989). Parts of the Grenville lithosphere have been reworked at that time. The plains to the west and north of the Grenville front are largely within a Proterozoic cratonic platform, in the Yavapai and Mazatzal provinces. These units were accreted during the Yavapai and Mazatzal orogenies (1.8–1.6 Ga) and have experienced little tectonic activity since then (Hoffman, 1988) (one exception is the Reelfoot Rift zone, a failed rift that was active 0.60–0.45 Ga ago (Ervin and McGinnis, 1975)).

The Appalachian region remained in the interior of the supercontinent Pangea until about 180 Ma, at which time rifting started to the East and the Atlantic Ocean began to open (Kazmin and Natapov, 1998; Beck and Housen, 2003). North America then began drifting NNW, a motion that continued until ~125 Ma (Kazmin and Natapov, 1998; Beck and Housen, 2003). At present, the absolute plate motion (APM) of North America is in the SE direction (azimuth 245°) at a rate of 2.6 cm/yr in the hotspot reference frame (Gripp and Gordon, 1990).

Seismic anisotropy has been detected throughout the area (e.g. Barruol et al., 1997; Fouch et al., 2000). The knowledge of the distribution of anisotropy at depth can help us constrain the history of deformation within the lithosphere and asthenosphere. The studies to date, however, have each mapped anisotropy in parts of but not the entire lithosphere–asthenosphere depth range, with results from different studies and different types of measurements complementary to one another in some instances but seemingly inconsistent with one another in other instances.

Shear-wave splitting observations in the eastern U.S. display a coherent large-scale pattern with the azimuth of fast wave propagation parallel to that of the APM (Fig. 2) (Barruol et al., 1997; Fouch et al., 2000). This can be interpreted as evidence for anisotropy in the asthenosphere due to the flow associated with the motion of the North American plate (Barruol et al., 1997; Fouch et al., 2000). The nearly uniform distribution of *SKS*-inferred fast-propagation azimuths thus may not, by itself, offer any information on lateral variations of anisotropy in the lithosphere.

Marone and Romanowicz (2007) combined surface-wave data and shear-wave splitting to constrain azimuthal anisotropy in the upper mantle beneath North America, and found two distinct anisotropic

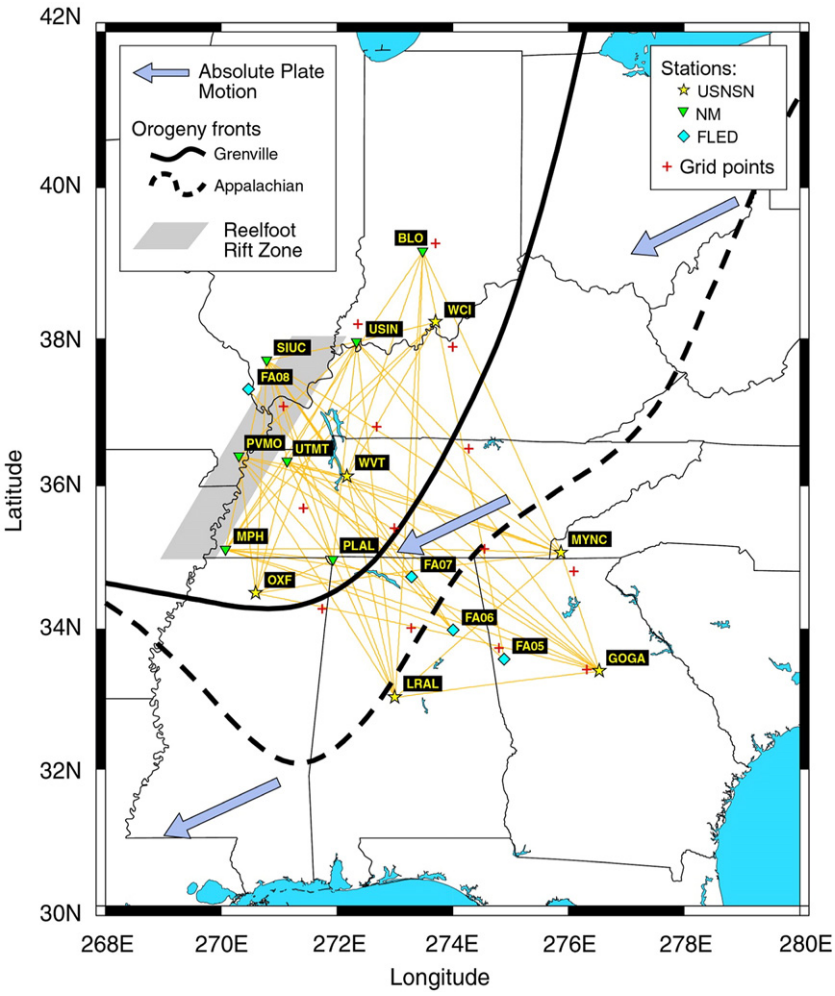

Fig. 1. The region of study and the interstation path coverage. The seismic stations used for the analysis are from both permanent and temporary networks (Deschamps et al., 2008). Red crosses show the grid knots at which we plot azimuthal anisotropy in Fig. 2; they belong to the grid used to parameterize the inversion for phase-velocity maps (Fig. 2). Grenville and Appalachian orogenic fronts are shown with a thick plain curve and a thick dashed curve, respectively. The Reelfoot Rift Zone is shown near the western boundary of the model area. Blue arrows indicate the absolute plate motion (APM) in the hotspot reference frame predicted by HS2-NUVEL1 (Gripp and Gordon, 1990). (For interpretation of the references to colour in this figure legend, the reader is referred to the web version of this article.)

layers, one in the lithospheric mantle, and another in the asthenosphere. Fast-propagation directions in the asthenosphere are parallel to the APM, in agreement with the inferences from *SKS* observations. Debayle et al. (2005), however, map only weak anisotropy in the asthenosphere beneath the eastern U.S. in their global model and argue that the rate of motion of North America and other continents, with the exception of Australia, is not sufficient to produce substantial anisotropy in the asthenosphere.

Smith and Ekström (1999) mapped azimuthal anisotropy of P_n waves which sample the uppermost mantle and found fast-propagation directions in the East-central U.S. that were roughly parallel to the Appalachian front (Fig. 2). This observation is consistent with pervasive deformation of the upper lithosphere (crust and uppermost mantle) to have occurred at the time of the Grenville and Appalachian orogenies. Marone and Romanowicz (2007) did not see this layer in their model because of the lack of surface-wave measurements at sufficiently short periods in their data set. Instead, they observed an anisotropic layer in the East-central U.S. lithosphere with a NNW-oriented fast-propagation azimuth, parallel neither to the APM nor to the Grenville and Appalachian fronts.

In this study we use broad-band, interstation measurements of Rayleigh-wave dispersion (Deschamps et al., 2008) and constrain the stratification of azimuthal anisotropy beneath the East-central U.S. in the entire lithosphere–asthenosphere depth range. Surface waves at different frequencies sample Earth structure at different depths. The frequency band of the measurements we use here is sufficiently broad (periods as short as 10 s to as long as 200 s) to resolve the layering of seismic structure and anisotropy from the crust down to the asthenosphere.

3. Layering of anisotropy

In a previous study (Deschamps et al., 2008), we have measured interstation phase-velocity curves for 60 pairs of stations in the East-central U.S. (Fig. 1) and constructed and validated anisotropic phase-velocity maps for the region. A robust phase-velocity curve was derived for each station pair by averaging over tens (up to over a hundred) of dispersion curves, each measured using the same station pair and signals from different earthquakes, normally in a number of different source regions (Meier et al., 2006). For all 60 paths, the period range includes the interval 18–34 s. For 33 paths the dispersion curve extends up to a period of 140 s, and for about 20 paths we could measure the dispersion curve up to a period of 200 s. In the phase-velocity maps, statistically significant azimuthal anisotropy with a π-periodic ("2Ψ") dependence of phase velocity on azimuth was detected (Smith and Dahlen, 1973). The resolution (averaging) lengths of the phase-velocity maps were estimated (Lebedev and Nolet, 2003) at ~210 km for isotropic anomalies and ~280 km for anisotropic

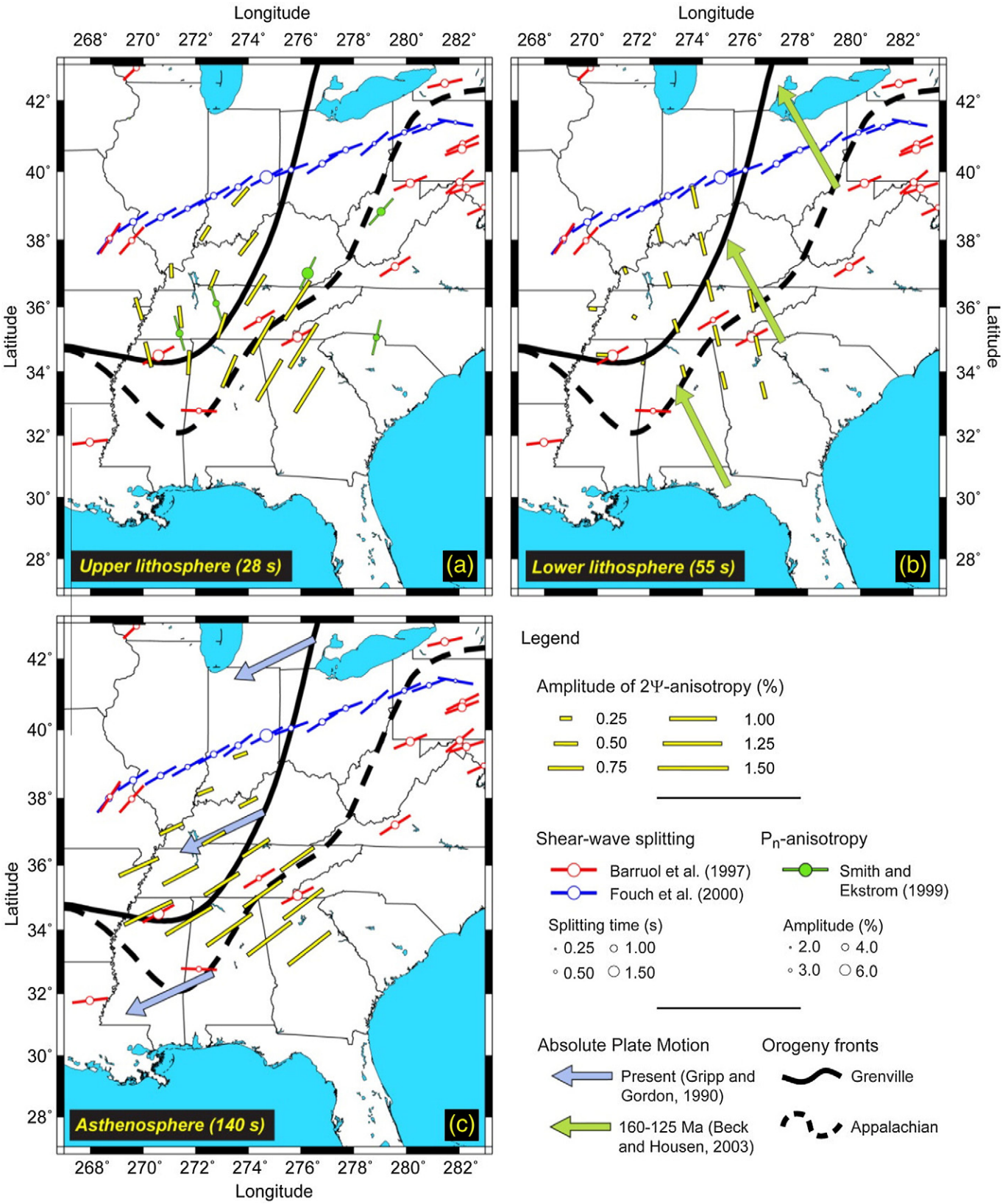

Fig. 2. Rayleigh wave azimuthal anisotropy (yellow bars) at 28, 55, and 140 s. The orientation and size of the bar show the direction of fastest propagation of Rayleigh waves at the period and the amplitude of the anisotropy, respectively. The isotropic average Rayleigh-wave velocities at 28, 55, and 140 s are 3.816, 4.053, and 4.337 km/s, respectively. Also plotted are main tectonic boundaries, past and present absolute plate motion, and previous anisotropy measurements. (a) At 28 s, the Rayleigh-wave fast-propagation direction beneath orogenic provinces is roughly parallel to the Grenville and Appalachian fronts, as well as to P_n fast-propagation direction (Smith and Ekström, 1999). (b) At 55 s, the fast-propagation azimuth is close to the direction of the NNW drift of the North American plate during the Mesozoic (Beck and Housen, 2003). (c) At 140 s, the fast-propagation direction is parallel to the current absolute plate motion (Gripp and Gordon, 1990), as well as to most fast-propagation directions inferred from shear-wave splitting observations in the area (Barruol et al., 1997; Fouch et al., 2000).

anomalies. Using Monte-Carlo sampling, errors in the amplitude of anisotropy and the fast-propagation azimuth were estimated at 8–10 m/s (i.e., 0.2–0.3% of the average isotropic velocity), and 15–20°, respectively, depending on the period (Deschamps et al., 2008).

Comparisons of dispersion curves for station-station pairs oriented at different azimuths strongly hinted at the occurrence of azimuthal anisotropy (Deschamps et al., 2008). The curve variability, however, also reflected isotropic heterogeneity. Inversions for phase-velocity maps have enabled us to separate anisotropic and isotropic signal; the presence of anisotropy in the models has been shown to be statistically significant (Deschamps et al., 2008). In this study we investigate further the depth distributions of *S*-velocity anisotropy and invert phase-velocity data for anisotropic point profiles as well as for region-average and path-average profiles. The results of these targeted inversions, together with the results of the phase-velocity analysis, allow us to derive robust conclusions regarding the layering of anisotropy and the evolution of the lithosphere–asthenosphere system.

3.1. Phase-velocity maps

Distributions of azimuthal anisotropy across the Rayleigh-wave phase-velocity maps (Deschamps et al., 2008) change gradually with the wave period. Within the period range 18–160 s they display distinctly different patterns in three period sub-ranges: 20–35 s, 50–60 s, and 100–160 s (between these sub-ranges patterns of anisotropy distributions gradually reshape one into the other). In Fig. 2 we plot azimuthal anisotropy at three representative periods (28, 55, 140 s), one within each of the three sub-ranges.

In the period range 20–35 s, phase-velocity azimuthal anisotropy is relatively strong (~1% of the isotropic average velocity) beneath the Grenville and Appalachian orogenic provinces, with the fast-propagation direction roughly parallel to the fronts (average azimuth is $\Psi_{\text{fast}}=32°$). Beneath the cratonic part of the region (eastern Yavapai and Mazatzal provinces) anisotropy is weaker (~0.6%) and has different and less coherent fast directions. Rayleigh waves at the 20–35 s periods sample primarily the lower crust and uppermost mantle. We infer that the anisotropy we observe indicates the fabric created in the upper lithosphere during the Grenville and Appalachian orogenies and frozen into the lower crustal and upper mantle rock ever since. According to Smith and Ekström (Smith and Ekström, 1999), the fast-propagation azimuth of P_n waves in the region is also parallel to the fronts, just as the Rayleigh-wave fast propagation azimuths mapped here (Fig. 2). The agreement between the patterns of anisotropy of Rayleigh waves (primarily sensitive to *S* velocities) around 28 s and P_n waves — both sample the uppermost mantle — reinforces the evidence for the occurrence of fabric oriented parallel to the orogeny fronts in the Grenville–Appalachian uppermost mantle.

In the period range 50–60 s, phase-velocity anisotropy is smaller (~0.5%), but the direction of fast propagation is laterally coherent. It is clearly different ($\Psi_{\text{fast}}=165°$) from that at shorter periods. Rayleigh waves at 50–60 s sample primarily mid-lower lithosphere, and we infer that no fabric created during the Grenville–Appalachian orogenies is apparent in this part of the lithosphere. Instead, the fast propagation direction is close to that of the paleo-APM, the direction of plate motion at 160–125 Ma according to plate-tectonic reconstructions (Beck and Housen, 2003). The anisotropy may thus indicate the fabric frozen into the lower lithosphere at those times, 160–125 Ma.

Around 140 s, phase-velocity azimuthal anisotropy is, again, stronger (>1%), and the direction of fast propagation is laterally uniform ($\Psi_{\text{fast}}=54°$) and parallel to the present APM direction (Gripp and Gordon, 1990). The anisotropy thus appears to be due to the strain associated with current and recent asthenospheric flow. Anisotropy is weaker beneath parts of the cratonic area (eastern Yavapai and Mazatzal provinces) in the North of our study region but is still present, with the same direction of fast propagation. The fast-propagation direction we mapped also matches the fast azimuths inferred from shear-wave splitting observations (Barruol et al., 1997; Fouch et al., 2000) (Fig. 2). This is consistent with an asthenospheric origin of most of the shear-wave splitting signal.

The anisotropic phase-velocity maps (Fig. 2) indicate that azimuthal anisotropy beneath the East-central U.S. is stratified into three layers. Anisotropic fabric within each layer appears to be of a different age, the age decreasing with increasing depth.

3.2. Inversion for shear-wave anisotropy

In order to investigate the stratification of shear-wave anisotropy more quantitatively, we now perform a series of inversions of phase-velocity data for anisotropic shear-velocity profiles. Using specific properties of anisotropic layering in the East-central U.S., we avoid complicated inversions for shear-velocity distributions with arbitrary depth-dependent azimuthal anisotropy and, instead, set up simple inversions for models that are approximate but sufficiently accurate for our purposes.

We observe that the fast-propagation direction at long periods (140 s) (Fig. 2) is nearly perpendicular to that at intermediate periods (55 s) and nearly parallel to that at short periods (28 s, Appalachian sub-region). We define a “fast” direction at an azimuth of 45°, close to the fast propagation azimuth at the long and short periods, and a “slow” direction perpendicular to it (135°, slow propagation at the long and short periods). Rayleigh waves at intermediate periods (50–60 s) will, in contrast to those at the long and short periods, travel faster at azimuth 135°, and slower at 45°. For any point, we can extract from the anisotropic phase-velocity maps a pair of “directional” dispersion curves containing phase velocities of Rayleigh waves propagating in the “fast” (45°) and the “slow” (135°) directions. At short and long periods, phase velocities will be higher in the “fast” direction, and at intermediate periods, higher in the “slow” direction.

A pair of such phase-velocity curves (the “fast” one and the “slow” one) can be inverted for a pair of shear-velocity profiles. We parameterize the inversion so as to solve simultaneously for an isotropic average profile and a profile of the amount of anisotropy, defined here as the difference in the speed of the shear waves that propagate in the “fast” and the “slow” directions. This inversion for the amount of anisotropy is approximate because our “slow” direction (135°) is not quite the same as the actual direction of fast Rayleigh-wave propagation at intermediate periods (165°). Even though the cosine function changes slowly near its maxima and minima, this difference will have an effect of reducing somewhat the difference between the fastest and slowest phase velocities at intermediate periods that go into the inversion, and, thus, will result in an underestimation of the amount of shear-wave anisotropy.

The inversion is non-linear and consists in a Gauss–Newton gradient search (from MATLAB optimization toolbox) parameterized with 15 boxcar and triangular functions that span a depth range from the upper crust down to a depth of 650 km. At each iteration, synthetic phase velocities are recomputed directly from shear-wave velocity profiles (Schwab and Knopoff, 1972) and compared to the ones according to our regional maps (Deschamps et al., 2008). The inversion minimizes the difference between the synthetic phase velocities and those from our maps. Compressional- and shear-velocity perturbations are coupled (δV_P (m/s)=δV_S (m/s)). Norm damping factor is applied independently to the isotropic and anisotropic terms. The Moho depth is also a free parameter of the inversion, and its damping is controlled by an independent parameter.

3.3. Anisotropic shear-wave profile at a point within the orogen

Fig. 3 illustrates the inversion and shows an anisotropic profile obtained for a point located in the orogenic part of the region (35.1°N, 274.5°E). The inversion was for the isotropic average profile (dashed black line, Fig. 3a) and for the profile of the amount of anisotropy,

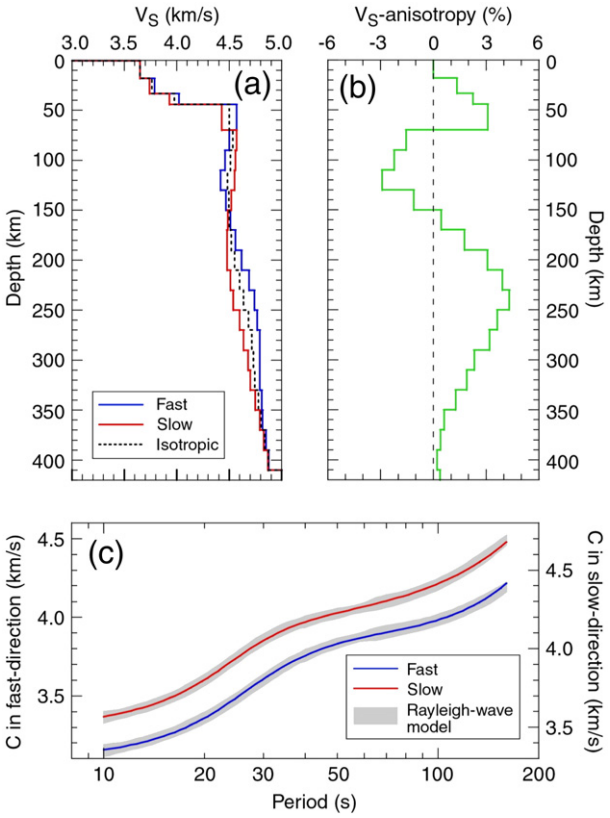

Fig. 3. Inversion for an anisotropic shear-wave velocity profile at a location within the orogenic part of the region (35.1°N, 274.5°E). (a) The dashed black curve shows the isotropic average V_S profile, the blue and red curves the speeds of the shear wave propagation in the "fast" and "slow" direction, respectively. (b) Anisotropic anomalies (difference between shear-wave propagation speeds at azimuths 45° and 135°) projected on the 45° azimuth. (c) Synthetic dispersion curves computed for the "fast" (blue) and "slow" (red) profiles (a). The gray shaded areas show the directional dispersion curves (extracted from the anisotropic phase-velocity maps and indicating phase velocities of Rayleigh waves at azimuths 45° and 135°) plus/minus the estimated error. (Note that the two dispersion curves are plotted using vertical axes shifted with respect to one another, each plotted on one side of the frame). (For interpretation of the references to colour in this figure legend, the reader is referred to the web version of this article.)

defined as the difference between shear speeds at the two azimuths, 45° and 135° (Fig. 3b). The blue and red profiles in Fig. 3a show the resulting shear-wave velocities in the "fast" and "slow" directions, respectively. Synthetic dispersion curves (Fig. 3c) computed for the best-fitting anisotropic shear-wave profile fit the dispersion curves extracted from the phase-velocity maps well within error bars (note that for clarity the fast and slow dispersion curves are plotted using vertical axes shifted with respect to one another, each plotted on one side of the frame).

If shear waves propagate faster at the azimuth 45° than at 135°, such anisotropy appears as positive on the profile in Fig 3b, if slower at 45° than at 135°, as negative. Three layers with distinctly different anisotropy are present at depths of about 15–70 km, 70–150 km, and below 150 km (beneath 250 km, the sensitivity of the phase-velocity data decreases, and the magnitude of decrease in anisotropy below this depth is not well constrained). The difference between the highest and lowest *S*-wave propagation speeds reach 2–3% within each of the three layers.

3.4. Region-average anisotropic shear-wave profiles

Taking $\Psi_{fast}=45°$ and $\Psi_{slow}=135°$, we have inverted pairs of the directional (at azimuths 45° and 135°) Rayleigh-wave phase-velocity curves simultaneously for isotropic average V_S profiles and profiles of anisotropy at each point of the model. We used phase-velocity maps in the period range 10–160 s (Deschamps et al., 2008). Fig. 4 shows the sub-region average profiles of the isotropic V_S (a) and of anisotropy (b) beneath the orogenic and cratonic areas.

Three anisotropic layers, associated with the Rayleigh-wave anisotropy observed at 20–35 s, 50–60 s and 140 s and higher, are clearly present beneath the orogenic part. In the upper lithosphere between the 30 km and 70 km depths, V_S anisotropy reaches 2.5% relative to isotropic V_S. In the 70–150 km depth range, anisotropy is with a direction of fastest V_S propagation nearly perpendicular to that in the layer above; the anisotropy reaches 2–2.5% and may be somewhat underestimated (see Section 3.2). Below ~150 km, anisotropy is, once more, with a faster wave propagation at the 45° azimuth, reaching 3–4% at 200–250 km. The pattern of anisotropy appears to change from a "frozen", lower-lithospheric one to an asthenospheric one near 150 km, indicating that the lithosphere–asthenosphere boundary (LAB), if it is identified to the mechanical boundary separating the rigid lithosphere from the deforming asthenosphere (Gung et al., 2003; Regan and Anderson, 1984), is currently located around this depth. The vertical resolution of our model does not allow us to estimate the sharpness of the LAB. A recent study using converted waves (Rychert et al., 2007), has indicated that the LAB beneath the Northeastern United States (NE of our study region) may be as sharp as 10 km in thickness.

V_S anisotropy averaged over the cratonic (Yavapai and Mazatzal) part of the region appears to be weaker than that beneath the orogen. In part, this is because of the greater variability in its fast-propagation directions, especially in the upper lithosphere (Fig. 2). Due to the smaller amplitude of anisotropy, it is difficult to estimate the depth of the LAB beneath the cratonic part of the region, although the profile (Fig. 4b) suggests that it may be somewhat deeper than beneath the orogen.

3.5. Anisotropic shear-wave profiles constrained with measured dispersion curves

The anisotropic phase-velocity maps (Section 3.1) are a result of regularized inversions of measured interstation dispersion curves (Deschamps et al., 2008). They are non-unique solutions of inverse problems, and this translates into an additional uncertainty on the shear-velocity profiles obtained in the following inversions (Section 3.2) in which we assume the maps to be data. In order to validate further our

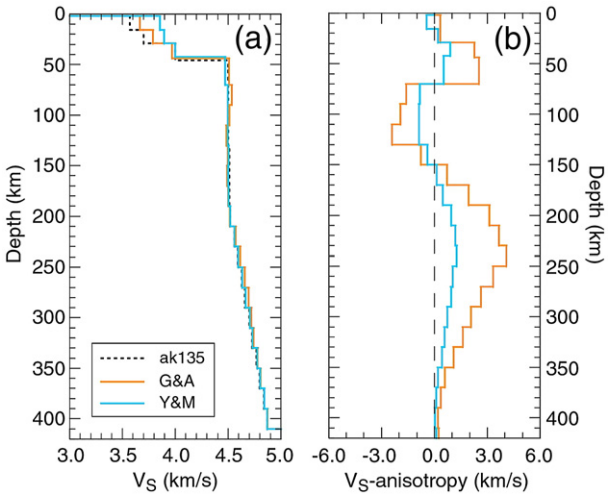

Fig. 4. (a) Average profiles of isotropic shear-wave velocity beneath the orogenic (orange curve) and cratonic (eastern Yavapai and Mazatzal provinces; blue curve) parts of the region. The black dashed curve is ak135 (Kennett et al., 1995). (b) Average V_S anisotropy beneath the orogenic (orange) and cratonic (blue) provinces (the difference between shear-wave propagation speeds at azimuths 45° and 135°). (For interpretation of the references to colour in this figure legend, the reader is referred to the web version of this article.)

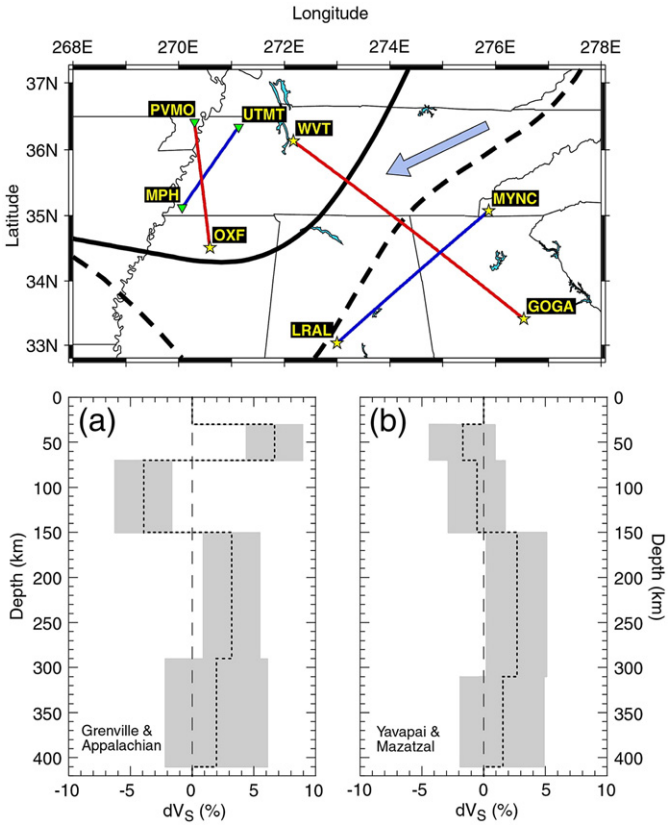

Fig. 5. Azimuthal anisotropy in the orogenic (a) and cratonic (eastern Yavapai and Mazatzal provinces) (b) parts of the region inferred from the inversion of selected pairs of measured dispersion curves. Monte-Carlo sampling was applied to radial V_S models that fit measured dispersion curves along 4 specially chosen paths (top map; see Fig. 1 for legend). The gray bands in plots a and b show probable anisotropy in the orogenic and cratonic regions and were defined by two standard deviations around the difference between a model obtained for a path striking near 45° and a model for a path striking near 135°. (a) Orogen: the paths are LRAL-MYNC (fast direction) and GOGA-WVT (slow direction). (b) Craton: the paths are MPH-UTMT (fast direction) and PVMO-OXF (slow direction).

conclusions regarding the layering of anisotropy, we now also invert selected measured dispersion curves directly for V_S profiles. Adopting a Monte-Carlo approach, we also aim to estimate the uncertainty of the anisotropic layering detected.

We choose one pair of station-station paths sampling primarily the orogenic part of the region (LRAL-MYNC and GOGA-WVT), and another pair of paths located in the cratonic part (MPH-UTMT and PVMO-OXF). The two paths in the orogenic part are nearly perpendicular to each other, one striking close to the direction of fast wave propagation at short and long periods, and the other close to the direction of slow propagation at short and long periods (but fast propagation at intermediate periods). The paths in the cratonic part (which, similarly to those within the orogen, were chosen both for their location and for the bandwidth of the corresponding dispersion curves) are also at a steep angle to one another, although not quite perpendicular. Of the four interstation paths, LRAL-MYNC and MPH-UTMT are thus at azimuths close the direction of fast wave propagation in the upper and lower anisotropic layers, and GOGA-WVT and PVMO-OXF are at azimuths nearly perpendicular to this direction.

In order to compute the average and standard deviation of the V_S profiles that fit the dispersion curves, we perform a Monte-Carlo search, generating a large (10^7) number of random V_S profiles. Each profile is constructed by an addition of random perturbations (up to 10%) in four layers (30–70 km, 70–150 km, 150–310 km, and 310–410 km) to the regional average profile. Computing a synthetic dispersion curve for each of these profiles, we compare it to the measured one and obtain the profile's probability p:

$$p(V_S) = ke^{-\frac{\chi^2}{2}}, \tag{1}$$

where

$$\chi^2 = \sum_j \frac{\Delta C_j^2}{\sigma_j^2} \tag{2}$$

and k is a normalization constant. ΔC_j is the difference between the calculated and measured phase velocity at period T_j, and σ_j is the uncertainty of the measurement at this period. Using these probabilities as weights, we then compute the weighted average and standard deviation of V_S, using the profiles that fit the data within twice the error bars.

The differences between the profiles obtained for LRAL-MYNC and GOGA-WVT and the profiles obtained for MPH-UTMT and PVMO-OXF are shown in Fig. 5a and b, respectively. Beneath the orogen (Fig. 5a), a three-layered profile of anisotropy with the direction of fast propagation in the intermediate layer nearly perpendicular to those in the upper and lower layers, is required in order to fit the measured dispersion curves. Beneath the cratonic part, anisotropy appears to be required only in the asthenospheric layer (150–310 km).

3.6. Agreement with shear-wave splitting observations

The fast shear-wave propagation direction in the asthenosphere derived from Rayleigh-wave data matches the fast-propagation directions inferred from *SKS*-splitting observations (Barruol et al., 1997; Fouch et al., 2000) (Fig. 2). This suggests that most if not all of the splitting may originate in the asthenosphere. Anisotropy in the upper lithosphere, where the fast-propagation directions in the orogenic part of the region are similar to those in the asthenosphere, may also contribute to the observed *SKS*-splitting signal.

In order to estimate the contribution of each anisotropic layer to the observed *SKS* splitting, we computed the times of the shear-wave splitting that would originate within each layer of our anisotropic models following Montagner et al. (2000) and Simons et al. (2002). In Table 1, we list the integrated splitting times (regional average and variance) for the three layers beneath both the orogenic and cratonic parts of the region. Beneath the orogen, the integrated shear-wave splitting time in the layer 30–70 km is about 0.2 s. This signal, however, may well be largely absent in the *SKS* waveforms due to anisotropy in the layer 70–150 km. The fast-propagation directions within the two layers are nearly perpendicular to one another, with similar amplitudes of their integrated splitting. Their contributions to the observed *SKS* splitting may thus balance one another. In the depth range 150–400 km, the integrated shear-wave splitting time reaches 1.1 s, in the range of the observed *SKS*-splitting values (Barruol et al., 1997; Fouch et al., 2000). Shear-wave splitting in this region can thus be accounted for by azimuthal anisotropy in the asthenosphere, the frozen fabrics in the upper layers contributing to the splitting only slightly. Thus, the conclusion that *SKS* splitting originates primarily in the asthenosphere does not preclude the presence of anisotropy in the lithosphere.

Table 1
Integrated shear-wave splitting that will originate in different layers beneath the orogenic (Grenville–Appalachian) and cratonic (Yavapai–Mazatzal) parts of the study region, according to the layering of anisotropy we have mapped $\langle \delta t \rangle$ and σ_{reg} are the regional average and variance, respectively

Layer	Orogenic terrains		Central plains	
	$\langle \delta t \rangle$ (s)	σ_{reg} (s)	$\langle \delta t \rangle$; (s)	σ_{reg} (s)
30–70 km	0.18	0.09	0.03	0.08
70–150 km	−0.20	0.08	−0.09	0.09
150–400 km	1.10	0.20	0.37	0.20

Beneath the cratonic part, the integrated splitting time estimates are smaller in all layers. Regarding the asthenospheric layer in particular, this apparent reduction in the magnitude of anisotropy in the northernmost part of our region may be surprising, given the fact that the shear beneath the moving North American plate should occur there as well as beneath the orogenic part, and the fact that the observed shear-wave splitting just north of the region sampled by our data is as strong as that in the east-central part of the region (Fig. 2). Whether the weakness of anisotropy we resolve may be due to a greater lithospheric thickness beneath the craton in the north of our study region, or due to complexities of asthenospheric flow caused by topography on the LAB, or simply due to the reduction in the resolving power of our data set in the northernmost part of the region will become clear in the future, when denser station coverage makes possible additional measurements of both surface-wave dispersion and *SKS* splitting.

4. Lithospheric evolution

The layered anisotropy beneath the Grenville–Appalachian orogen reflects the history of deformation of its lithosphere over the last few hundred million years. Anisotropic fabric in the upper lithosphere (~25–70 km) with a direction of fast wave propagation parallel to the Grenville and Appalachian fronts, as indicated both by S-wave azimuthal anisotropy mapped in this study and by P_n-wave azimuthal anisotropy (Smith and Ekström, 1999). This represents evidence for pervasive deformation of the upper lithosphere, including lithospheric mantle, during the continental collisions, with front-parallel extension (Silver, 1996; Meissner et al., 2002). After the end of the Appalachian orogeny (~270 Ma), the region has not experienced major tectonic activity, and the anisotropic fabric has remained frozen in the upper lithosphere.

By the end of the Appalachian orogeny, the lithosphere is likely to have been at least 70 km thick. The fabric within the 70-km thick upper lithosphere is preserved to this day, whereas in the deeper lithosphere the fabric is different, probably unrelated to the orogeny. One may contemplate a scenario in which the lithosphere was thicker than 70 km but was easily deformable and unable to preserve the fabric below 70 km. Such behavior, however, would make this deep deformable layer essentially asthenospheric, at least from a rheological point of view.

The direction of fast wave propagation in the 70–150 km depth range is parallel neither to the orogenic fronts, nor to the direction of the present absolute plate motion (APM). Instead, it is parallel to the direction of paleo-APM, the NNW motion of the North American plate at ~160–125 Ma. The fabric in the 70–150 km depth range may thus be of that age, 160–125 Ma.

In the recent times, the lower lithosphere beneath the Grenville–Appalachian orogen in the East-central US must not have experienced substantial deformation in the depth interval 70–150 km. It preserves anisotropic fabric that is distinctly different from that found in the asthenosphere below ~150 km depth. It thus appears likely that the

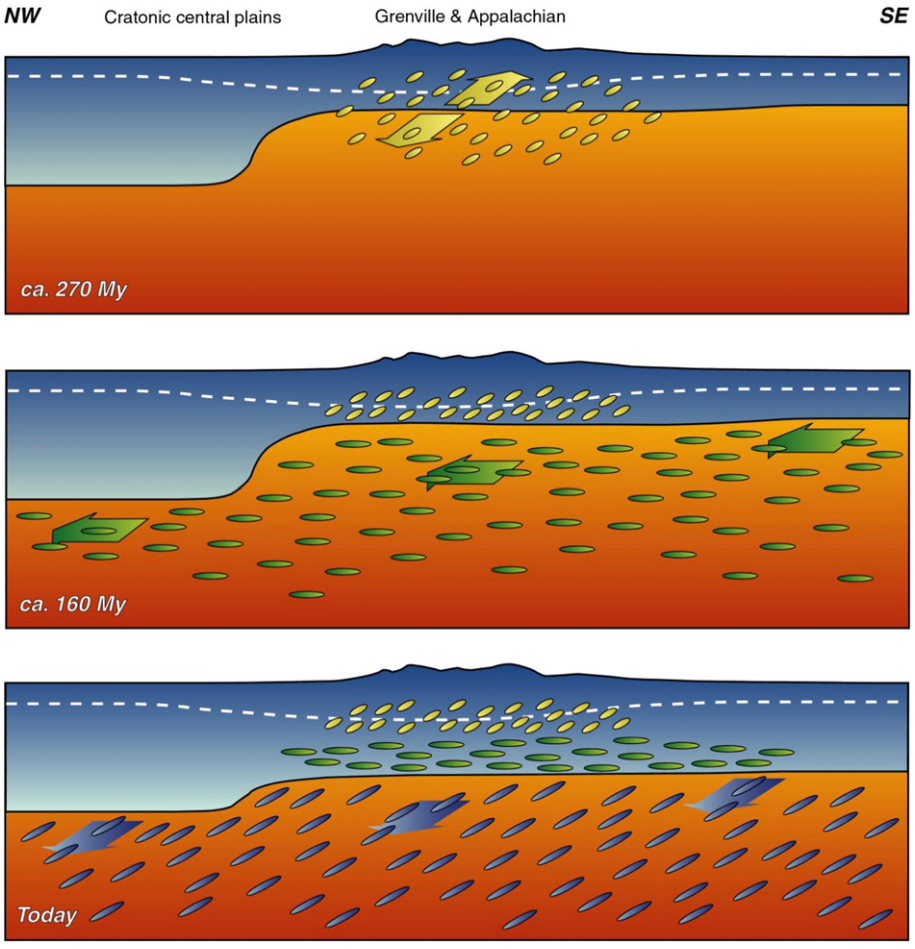

Fig. 6. A possible scenario for the origin of anisotropic layering beneath the East-central United States. During the Appalachian orogeny (up to 270 My), pervasive deformation occurred in the lower crust and lithospheric mantle. By the end of the orogeny, the lithosphere was 70 km thick. The warm, deformable material below 70 km then cooled down. Between 160 and 125 Ma, the lithosphere thickened. The lower lithosphere inherited the fabric from the asthenosphere below (of which it was forming); the fabric trended NNW, parallel to the direction of then plate motion. The two episodes of deformation resulted in two layers of frozen seismic anisotropy beneath the orogen. Today, the motion of the North American plate induces deformation giving rise to seismic anisotropy in the asthenosphere.

lithosphere has grown in thickness, from 70 km thick immediately after the Appalachian orogeny to 150 km thick at present. As it was thickening, the lower lithosphere has inherited the fabric of the sheared asthenosphere below (Fig. 6). This would explain why the fabric frozen into the lower lithosphere is characterized by a fast wave-propagation direction parallel to the azimuth of the plate motion at 160–125 Ma.

To investigate this scenario further, we modelled the diffusive cooling of a thickening lithosphere (Fig. 7). We solved the equation of diffusion in one dimension with a constant thermal diffusivity ($\kappa = 10^{-6}$ m^2/s) using an implicit finite-differences scheme. At time $t=0$, we imposed a temperature $T_m = 1300$ °C everywhere between $z=70$ and $z=220$ km. Between the surface and $z=70$ km, the initial geotherm is computed following Chapman (1986) and a surface heat flux equal to 60 mW/m^2. The whole layer is then cooled down by imposing the surface and bottom temperatures, $T_{surf}=0$ and $T_{220}=T_m=1300$ °C, respectively. We have then computed the differential stress (strength envelop) following the approach of Kohlstedt et al. (1995). We assumed a non-Newtonian relationship between strain rate and differential stress with stress exponent $n=3.6$, and activation energy $Q=535$ kJ/mol. We neglected the effects of grain size and water. According to this model, a 150 km thick layer that is initially at mantle temperature will thermally relax in about 150 Ma. Interestingly, the observed fast-propagation direction in the lower lithosphere is roughly parallel to the reconstructed plate motion at 160–125 Ma, i.e. up to 150 Ma after the end of the Appalachian orogeny. By the end of this episode the material would have already cooled down substantially, which may have limited the amount of any subsequent deformation and preserved then existing anisotropic fabric frozen in this layer. This scenario provides a coherent explanation for the presence of two layers of frozen anisotropy, but is mainly qualitative. In addition, it refers to the thermal lithosphere, which is only a good proxy for the mechanical lithosphere if the root is not affected by chemical depletion. Chemical differentiation may, however, have played a key role in the lithospheric growth. Recent analogue experiments and stability analysis (Jaupart et al., 2007) suggest that continental lithosphere is close to the instability of thermochemical convection, and may have grown by successive episodes of oscillatory convection. Further geodynamical modeling of root removal (or extrusion) and lithospheric growth, including thermochemical convection and an extensive exploration of the lithospheric-cooling model space (initial geotherm, radiogenic heating, thermal diffusity) would be needed to built a more quantitative scenario.

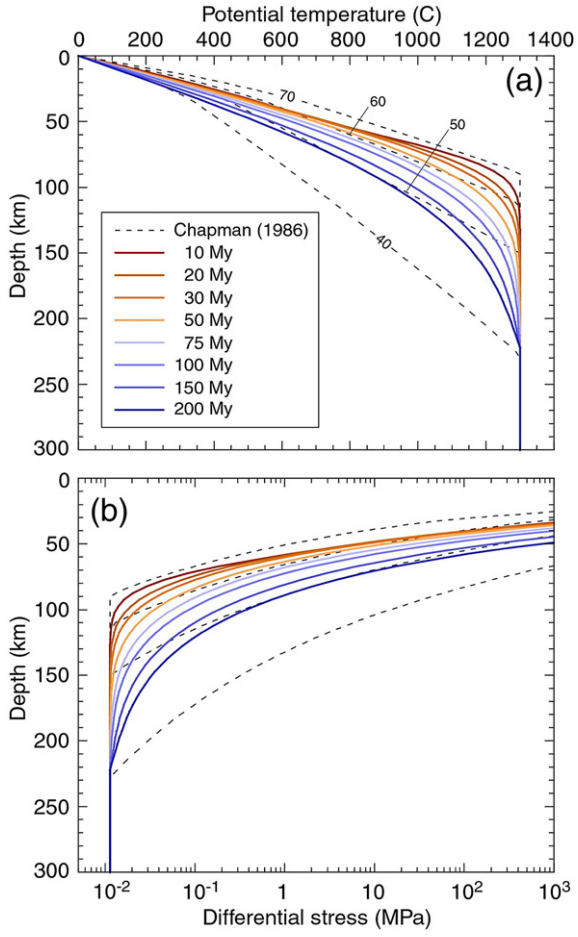

Fig. 7. (a) Diffusive cooling of a 150 km layer initially at mantle temperature. The thermal diffusivity is constant and equal to 10^{-6} m^2/s. For comparison, the dotted profiles show Chapman's geotherms for surface heat flux equal to 40, 50, 60 and 70 mW/m^2 (Chapman, 1986). The initial temperature profile is computed according to Chapman with a surface heat flux equal to 60 mW/m^2. At $t=0$, a temperature $T_m=1300$ °C is imposed between $z=70$ km and $z=220$ km. The system then starts to cool down, as shown by the series of temperature profiles. At $t=150$ My, the temperature profile is close to the Chapman's geotherm for $q_s=50$ mW/m^2, which is typical of stable platforms (Rohm et al., 2000). (b) Lithospheric strength envelopes (differential stress) computed for each of the temperature profile in plot (a). Following Kohlstedt et al. (1995), we assumed a non-Newtonian relationship between the strain rate and the differential stress, with a stress exponent $n=3.6$, and an activation energy $Q=535$ kJ/mol. Lithosphere gets stronger as it cools down.

Anisotropy in the deepest anisotropic layer we detect, below 150 km, appears to be due to current and recent asthenospheric flow. The direction of fast wave propagation is parallel to the current and recent APM. Simple shear in the asthenosphere due to the relative lithosphere–asthenosphere motion deforms mantle minerals. Given sufficient finite strain, olivine, the most abundant mineral in the upper mantle, develops preferred orientation in the direction of the flow, which results in seismic anisotropy (e.g. Karato, 1998). We have shown that the anisotropy we detect can account for published shear-wave splitting observations, both the fast-propagation directions and the splitting times. With continent-scale tomography, Marone and Romanowicz (2007) have also recently mapped asthenospheric anisotropy beneath eastern North America with fast-propagation directions parallel to the APM, and also pointed out that surface-wave and *SKS*-splitting observations are compatible. This consistency is further evidence for the plate-motion related anisotropy in the asthenosphere.

5. Conclusions

We have constrained the stratification of azimuthal anisotropy in the entire lithosphere–asthenosphere depth range beneath the Grenville–Appalachian orogen in the East-central U.S. Anisotropic patterns in parts of this depth range have been detected in the region previously, displaying different directions of fast wave propagation: parallel to tectonic trends, parallel to the current plate-motion direction, or not parallel to either (Marone and Romanowicz, 2007; Barruol et al., 1997; Fouch et al., 2000; Smith and Ekström, 1999).

Here we show that three distinct layers with different anisotropic fabric within each are present. The upper lithosphere (30–70 km depth range) is characterized by fast-propagation directions parallel to the Grenville and Appalachian fronts. We interpret this anisotropy as an indication of fabric frozen within the lower crust and uppermost mantle since the time of the Appalachian orogeny (>270 Ma). The lower lithosphere (70–150 km) displays fabric with a NNW fast-propagation direction. This is parallel to the direction of the North America plate motion at 160–125 Ma, and we infer that that is the age of the lower-lithospheric fabric. The asthenosphere (>150 km) shows anisotropic fabric with the direction of fast wave propagation parallel to the direction of the current plate motion; this fabric, apparently, is due to current and recent strain in the asthenosphere.

The layering of seismic anisotropy yields important new information regarding the history of deformation and evolution of the lithosphere. The front-parallel pattern of anisotropy in the uppermost

mantle and its occurrence at a scale of hundreds of kilometers (as shown by both surface-wave and P_n analyses) are evidence for pervasive, distributed deformation of the entire lithosphere at the time of the orogenies. The lithosphere appears to have been 70 km thick by the completion of the Appalachian suturing, because the fabric that is, apparently, associated with the orogeny is found above but not below 70 km. At present, the lithosphere is likely to be ~150 km thick, because below 150 km the fabric trends parallel to the present plate-motion direction, probably an expression of current and recent deformation in the asthenosphere, and above 150 km the fabric is oriented differently and appears to be fossil.

Post-orogenic evolution of the lithosphere has thus included substantial thickening, likely to have occurred by "freezing" of asthenospheric material onto the bottom of moving lithosphere. Because the fabric found in the lower lithosphere trends parallel to the plate motion at 160–125 Ma, much of the thickening of the lithosphere must have occurred at that time, with the new lithosphere inheriting the fabric from the sheared asthenosphere below, from which it was forming.

Acknowledgments

We are grateful to Thorsten Becker and Barbara Romanowicz for their insightful, constructive reviews.

References

Barruol, G., Silver, P.G., Vauchez, A., 1997. Seismic anisotropy in the eastern United States: deep structure of a complex continental plate. J. Geophys. Res. 102, 8329–8348.
Beck, M.E., Housen, B.A., 2003. Absolute velocity of North America during the Mesozoic from paleomagnetic data. Tectonophysics 377, 33–54.
Becker, T.W., Chevrot, S., Schulte-Pelkum, V., Blackman, D.K., 2006. Statistical properties of seismic anisotropy predicted by upper mantle geodynamic model. J. Geophys. Res. 111. doi:10.1029/2005JB004095.
Becker, T.W., Browaeys, J.T., Jordan, T.H., 2007. Stochastic analysis of shear-wave splitting length scales. Earth Planet. Sci. Lett. 259, 526–540.
Chapman, D.S., 1986. Thermal gradients in the continental crust. In: Dawson, J.B., Carswell, D.A., Hall, J., Wedepohl, K.H. (Eds.), The nature of the continental crust. Spec. Publ. Geol. Soc. London, vol. 24, pp. 63–70.
Christensen, N.I., 1984. The magnitude, symmetry and origin of upper mantle anisotropy based on fabric analyses of ultramafic tectonics. Geophys. J. R. Astron. Soc. 76, 89–112.
Dalziel, I.W.D., 1991. Pacific margins of Laurentia and East Antarctica–Australia as a conjugate rift pair: evidences and implications for an Eocambrian supercontinent. Geology 19, 598–601.
Debayle, E., Kennett, B.L.N., Priestley, K., 2005. Global anisotropy and the thickness of continents. Nature 433, 509–512.
Deschamps, F., Lebedev, S., Meier, T., Trampert, J., 2008. Azimuthal anisotropy of Rayleigh-wave phase velocities in the east-central United States. Geophys. J. Int. 173, 827–843.
Dickinson, W.R., 1971. Plate tectonics in geologic history. Science 174, 108–113.
Ervin, C.P., McGinnis, L.D., 1975. Reelfoot rift: reactivated precursor to the Mississippi embrayement. Geol. Soc. Am. Bull. 86, 1287–1295.
Fischer, K.M., Wiens, D.A., 1996. The depth distribution of mantle anisotropy beneath the Tonga subduction zone. Earth Planet. Sci. Lett. 142, 253–260.
Forsyth, D.W., 1975. The early structural evolution and anisotropy of the oceanic upper mantle. Geophys.J. R. Astron. Soc. 43, 103–162.
Fouch, M.J., Rondenay, S., 2006. Seismic anisotropy beneath stable continental interiors. Phys. Earth Planet. Inter. 158, 292–320.
Fouch, M.J., Fischer, K., Parmentier, E.M., Wysession, M.E., Clarke, T.J., 2000. Shear-wave splitting, continental keels, and patterns of mantle flow. J. Geophys. Res. 105, 6255–6275.
Gaherty, J.B., Jordan, T.H., 1995. Lehmann discontinuity as the base of an anisotropic layer beneath continents. Science 268, 1468–1471.
Gripp, A.E., Gordon, R.G., 1990. Current plate velocities relative to the hotspots incorporating the NUVEL-1 global plate motion model. Geophys. Res. Lett. 17, 1109–1112.
Gung, Y., Panning, M., Romanowicz, B., 2003. Global anisotropy and the thickness of continents. Nature 422, 707–711.
Hoffman, P.F., 1988. United Plates of America, the birth of a craton. Early Proterozoic assembly and growth of Laurentia. Ann. Rev. Earth Planet. Sci. 16, 543–603.
Jaupart, C., Molnar, P., Cottrell, E., 2007. Instability of a chemically dense layer heated from below and overlain by a deep less viscous fluid. J. Fluid Mech. 572, 433–469.
Karato, S., 1998. Seismic anisotropy in the deep mantle, boundary layers, and the geometry of mantle convection. Pageoph 151, 565–587.
Karlstrom, K.E., Åhäll, K.I., Harlan, S.S., Williams, M.L., McLelland, J., Geissman, J.W., 2001. Long-lived (1.8–1.0 Ga) convergent orogen in southern Laurentia, its extension to Australia and Baltica, and implications for refining Rodinia. Precambrian Res. 111, 5–30.
Kazmin, V.G., Natapov, L.M. (Eds.), 1998. Paleogeographic Atlas of Northern Eurasia. Institute of Tectonics of Lithospheric Plates, Moscow. CD-ROM.
Kennett, B.L.N., Engdahl, E.R., Buland, R., 1995. Constraints on seismic velocities in the Earth from traveltimes. Geophys. J. Int. 122, 108–124.
Kohlstedt, D.L., Evans, B., Mackwell, S.J., 1995. Strength of the lithosphere: constraints imposed by laboratory experiments. J. Geophys. Res. 100, 17587–17602.
Lebedev, S., Nolet, G., 2003. Upper mantle beneath southeast Asia from S velocity tomography. J. Geophys. Res. 108. doi:10.1029/2000JB000073.
Li, A., Forsyth, D.W., Fischer, K.M., 2003. Shear velocity structure and azimuthal anisotropy beneath North America from Rayleigh-wave inversion. J. Geophys. Res. 108. doi:10.1029/2002JB002259.
Marone, F., Romanowicz, B., 2007. The depth distribution of azimuthal anisotropy in the continental upper mantle. Nature 447, 198–203.
McClusky, A., Blassanian, S., Barka, A., et al., 2000. Global positioning system constrains on plate kinematics and dynamics in the eastern Mediterranean and Caucasus. J. Geophys. Res. 105, 5695–5719.
Meier, T., Dietrich, K., Stöckhert, B., Harjes, H.P., 2006. One-dimensional model of shear wave velocity for the eastern Mediterranean obtained from the inversion of Rayleigh-wave phase velocities and tectonic implications. Geophys. J. Int. 156, 45–58.
Meissner, R., Mooney, W., Artemevia, I., 2002. Seismic anisotropy and mantle creep in young orogens. Geophys. J. Int. 149, 1–14.
Meissner, R., Rabbel, W., Kern, H., 2006. Seismic lamination and anisotropy of the Lower Continental Crust. Tectonophysics 416, 81–99.
Molnar, P., 1988. Continental tectonics in the aftermath of plate tectonics. Nature 335, 131–137.
Molnar, P., Anderson, H., Audoine, E., Eberhart-Phillips, D., Gledhill, K., Klosko, E., McEvilly, T., Okaya, D., Savage, M., Stern, T., Wu, F., 1999. Continuous deformation versus faulting through continental lithosphere: tests using New Zealand as a laboratory for the study of continental dynamics. Science 286, 516–519.
Montagner, J.P., Griot-Pommera, D.A., Lave, J., 2000. How to relate body wave and surface wave anisotropy? J. Geophys. Res. 105, 19,015–19,027.
Nicolas, A., Christensen, N.I., 1987. Formation of anisotropy in upper mantle peridotites — a review. In: Fuchs, K., Froidevaux, C. (Eds.), Composition, structure and dynamics of the Lithosphere–Asthenosphere system, pp. 111–123.
Nishimura, C.E., Forsyth, D.W., 1989. The anisotropic structure of the upper mantle in the Pacific. Geophys. J. Int. 96, 203–229.
Pedersen, H.A., Bruneton, M., Maupin, V., SVEKALAPKO Seismic Tomography Working group, 2006. Lithospheric and sublithospheric anisotropy beneath the Baltic shield from surface-wave array analysis. Earth Planet. Sci. Lett. 244, 590–605.
Regan, J., Anderson, D.L., 1984. Anisotropic models of the upper mantle. Phys. Earth Planet. Inter. 35, 227–263.
Rohm, A., Snieder, R., Goes, S., Trampert, J., 2000. Thermal structure of continental upper mantle inferred from S-wave velocity and surface heat flow. Earth Planet. Sci. Lett. 181, 395–407.
Rychert, C.A., Rondenay, S., Fischer, K.M., 2007. P-to-S and S-to-P imaging of a sharp lithosphere–asthenosphere boundary beneath eastern North America. J. Geophys. Res. 112. doi:10.1029/2006JB004619.
Savage, M.K., 1999. Seismic anisotropy and mantle deformation: what we have learned from shear-wave splitting. Rev. Geophys. 37, 65–106.
Schwab, F., Knopoff, L., 1972. Fast surface wave and free mode computations. In: Bolt, B.A. (Ed.), Method in Compotational Physics, vol. 11. Academic Press, New-York.
Sebai, A., Stutzmann, E., Montagner, J.P., Sicilia, D., Beucler, E., 2006. Anisotropic structure of the African upper mantle from Rayleigh and Love wave tomography. Phys. Earth Planet. Inter. 155, 48–62.
Silver, P.G., 1996. Seismic anisotropy beneath the continents: probing the depths of geology. Annu. Rev. Earth Planet. Sci. 24, 385–432.
Simons, F.J., van der Hilst, R.D., Montagner, J.P., Zielhuis, A., 2002. Multimode Rayleigh-wave inversion for heterogeneity and azimuthal anisotropy of the Australian upper mantle. Geophys. J. Int. 151, 738–754.
Sleep, N.H., 2005. Evolution of the continental lithosphere. Annu. Rev. Earth Planet. Sci. 33, 369–393.
Smith, G.P., Ekström, G., 1999. A global study of *Pn*-anisotropy beneath continents. J. Geophys. Res. 104, 963–980.
Smith, M.L., Dahlen, F.A., 1973. The azimuthal dependence of Love- and Rayleigh-wave propagation in a slightly anisotropic medium. J. Geophys. Res. 78, 3321–3333.
Smith, D.B., Ritzwoller, M.H., Shapiro, N.M., 2004. Stratification of anisotropy in the Pacific upper mantle. J. Geophys. Res. 109. doi:10.1029/2004JB003200.
Tapponnier, P., Xu, Z.Q., Roger, F., Meyer, B., Arnaud, N., Wittlinger, G., Yang, J.S., 2001. Oblique stepwise rise and growth of the Tibet Plateau. Science 294, 1671–1677.
Tatham, D.J., Lloyd, G.E., Butler, R.W.H., Casey, M., 2008. Amphibole and lower crustal seismic properties. Earth Planet. Sci. Lett. 267, 118–128.
Vinnik, L.P., Kosarev, G.L., Makeyeva, L.I., 1984. Anisotropy of the lithosphere from the observations of SKS and SKKS. Proc. Acad. Sci. USSR Geol. Sci. Sect., Engl. Transl.
Vinnik, L.P., Makeyeva, L.I., Milev, A., Usenko, A., 1992. Global patterns of azimuthal anisotropy and deformations in the continental mantle. Geophys. J. Int. 111, 433–447.
Yang, Y., Forsyth, D.W., 2006. Rayleigh-wave phase velocities, small-scale convection, and azimuthal anisotropy beneath southern California. J. Geophys. Res. 111. doi:10.1029/2005JB004180.
Yao, H., van der Hilst, R.D., de Hoop, M.V., 2006. . Surface-wave array tomography in SE Tibet from ambient seismic noise and two-station analysis — I. Phase velocity maps. Geophys. J. Int. 166, 732–744.
Zhang, P.Z., Shen, Z.K., Wang, M., Gan, W.J., Bürgmann, R., Molnar, P., Wang, Q., Niu, Z.J., Sun, J.Z., Wu, J.C., Hanrong, S., Xinzhao, Y., 2004. Continuous deformation of the Tibetan Plateau from global positioning system data. Geology 32, 809–812.
Zhang, X., Paulssen, H., Lebedev, S., Meier, T., 2007. Surface wave tomography of the Gulf of California. Geophys. Res. Lett. 34. doi:10.1029/2007GL030631.
Ziegler, P.A., 1989. Evolution of Laurussia: A Study in Late Paleozoic Plate Tectonics. Kluwer Academic Publishers, Dordrecht. 102 pp.